Predicting the Terminal Solid Solubility of Hydrogen in Zirconium Using the Phase-Field Method

Sanghyun Ji [a], Kunok Chang[a]**
[a]*Department of Nuclear Engineering, Kyung Hee University, Yong-in city, Republic of Korea*
[*]*Corresponding author: kunokchang@khu.ac.kr*

***Keywords :** Zirconium, Zirconium hydride, Terminal solid solubility

1. Introduction

During reactor operation, the outer side of the zirconium cladding undergoes uniform oxidation, producing hydrogen as a byproduct, part of which diffuses into the cladding through the oxide layer [1]. When the local hydrogen concentration exceeds the solubility limit, zirconium hydrides start to precipitate. The precipitated hydrides could compromise the mechanical integrity of the zirconium cladding not only by causing cladding embrittlement, but also by promoting the formation of blisters of hydrides and crack initiation sites, which could increase the risk of cladding failure. Therefore, an accurate determination of the hydrogen solubility limit in zirconium is essential for nuclear fuel performance and safety assessment, because the solubility of hydrogen defines the conditions when the precipitation and dissolution of hydrides occur.

The terminal solid solubility of hydrogen (TSS) is defined as the maximum amount of hydrogen that can be retained in solid solution without forming hydride precipitates, and experimental studies revealed a pronounced thermal hysteresis between hydride precipitation and hydride dissolution, giving rise to two distinct solubility limits: TSSP determined during cooling and TSSD determined during heating [2].

Although the origin of hysteresis is under debate, multiple studies have reported that elastic strain energy and plastic deformation contribute to the precipitation and dissolution of hydrides. However, it is difficult to exclusively and quantitatively evaluate the individual contributions of interfacial energy, elastic strain energy, and plastic deformation based on experiments alone.

Therefore, a computational approach capable of resolving these coupled thermodynamic and mechanical effects within a self-consistent framework is required. In this study, we focus on the δ-hydride phase, and the objective of this work is to quantitatively assess the effects of interfacial energy, elastic strain energy, and plastic deformation on hydride precipitation and dissolution in α-zirconium

2. Methods

To perform numerical simulations of microstructural evolution during phase transformation while incorporating both thermodynamic energy and mechanical energy, the phase-field method was adopted. Among phase-field formulations, the Kim–Kim–Suzuki (KKS) model was adopted because it enforces local chemical equilibrium across diffuse interfaces by requiring equality of the chemical potentials in the α-zirconium matrix and the δ hydride phase, allowing the concentration partitioning to be determined directly from the underlying free energy functions [3].

2.1 Governing equations

In the phase-field model, each phase is represented by an order parameter η, which continuously varies from 0 to 1 at the interface. In our work, η = 0 corresponds to the α-zirconium phase and η = 1 to the δ -hydride phase. The spatial and temporal evolution of η describes the phase transformation process, while the composition field c represents the concentration of hydrogen.

For the non-conserved order parameter η, we solved the Allen–Cahn equation, Eq. 1.

$$\frac{\partial \eta}{\partial t} = -L_{\eta}\frac{\delta F_{Total}}{\delta \eta} \quad (1)$$

Here, L_{η} is the kinetic coefficient associated with interface mobility, and $\frac{\delta F_{Total}}{\delta \eta}$ is the functional derivative of the total free energy F with respect to the order parameter η. In this work, we set L_{η} = 1 to guarantee a diffusion-controlled process.

For the conserved concentration field c, the Cahn–Hilliard equation, Eq. 2, was used to describe the evolution of the hydrogen concentration while conserving the total hydrogen content.

$$\frac{\partial c}{\partial t} = \nabla \cdot \left(M_{c} \nabla \frac{\delta F_{Total}}{\delta c} \right) \quad (2)$$

Here, M_{c} is the mobility of hydrogen, $\frac{\delta F_{Total}}{\delta c}$ is the functional derivative of the total free energy F_{Total} with respect to the concentration of hydrogen.

2.2 Free energy

The total free energy F_{Total} used to model hydride precipitation and dissolution is composed of three contributions, as shown in Eq. 3. Here, f_{chem}, f_{int}, and $f_{elastic}$ denote the chemical, interfacial, and elastic free energy densities.

$$F_{Total} = \int_V (f_{chem} + f_{int} + f_{elastic})dV \quad (3)$$

In Eq. 3, the chemical free-energy density f_{chem} is defined in Eq. 4 as an interpolation of the α-zirconium and δ-hydride free-energy densities, with the phase-specific thermodynamic functions taken from a CALPHAD-based thermodynamic database.

$$f_{chem} = \big(1 - h(\eta)\big)f_\alpha(c_\alpha, T) + h(\eta)f_\delta(c_\delta, T) \quad (4)$$

Here, f_α and f_δ denote the CALPHAD-based free-energy densities of the α-zirconium and δ-hydride phases. The interpolation function $h(\eta)$ is defined as a smooth polynomial, as shown in Eq. 5.

$$h(\eta) = \eta^3(6\eta^2 - 15\eta + 10) \quad (5)$$

The global hydrogen concentration is related to the phase concentrations through Eq. 6.

$$c = \big(1 - h(\eta)\big)c_\alpha + h(\eta)c_\delta \quad (6)$$

Local chemical equilibrium across the diffuse interface is enforced by equality of diffusion potentials, as shown in Eq. 7.

$$\frac{\partial f_\alpha}{\partial c_\alpha} = \frac{\partial f_\delta}{\partial c_\delta} \quad (7)$$

This condition ensures thermodynamic consistency by satisfying the CALPHAD-based chemical potentials of the two phases at the interface.

The precipitation of hydride generates significant strains because the molar volume of the δ-hydride differs from that of the α-zirconium matrix, which induces strong local stresses around the precipitates. The elastic strain energy density is expressed as Eq. 8.

$$f_{elastic} = \frac{1}{2}C_{ijkl}(r)\epsilon_{ij}^{el}(r)\epsilon_{kl}^{el}(r) \quad (8)$$

The stiffness tensor is treated as phase dependent and is smoothly interpolated across the diffuse interface using the switching function $h(\eta)$, as shown in Eq. 9.

$$C_{ijkl}(r) = \big(1 - h(\eta)\big)C_{ijkl}^{\alpha}(r) + h(\eta)C_{ijkl}^{\delta}(r) \quad (9)$$

The elastic strain is defined by subtracting the stress-free strain (eigenstrain) from the total strain), as shown in Eq. 10.

$$\epsilon_{ij}^{el}(r) = \epsilon_{ij}^{total}(r) - \epsilon_{ij}^{0}(r) \quad (10)$$

An elastic-only description is not sufficient to reproduce the TSSP, because part of the strain is relaxed by plastic deformation. To incorporate this effect, a relaxation factor ψ is introduced, as shown in Eq. 11.

$$\epsilon_{ij}^{0}(r) = \big(1 - h(\eta)\big)\epsilon_{ij}^{\alpha}(r) - (1 - \psi)h(\eta)\epsilon_{ij}^{\delta}(r) \quad (11)$$

In this formulation, ψ is introduced to represent the effective stress relaxation associated with plastic deformation by reducing the transformation strain contribution of the δ-hydride. In the present study, ψ is determined at each temperature by calibrating it so that the simulated precipitation threshold matches the experimentally measured TSSP, which yields a temperature-dependent $\psi(T)$.

2.3 Simulation details

The simulation was conducted in a two-dimensional α-zirconium matrix with a size of 1024 nm $\times$ 1024 nm, and periodic boundary conditions were applied to both the order parameter $\eta$and hydrogen concentration c in all directions to represent an effectively infinite medium and minimize boundary effects.

For dissolution simulations, a single spherical δ-hydride particle was placed at the center of the domain. Simulations were conducted at $T = 500$, 550, 600, and 650 K, for interfacial energies of 0.623, 1.247, 1.871 eV/nm^2. The particle radii of $r = 4$, 6, 8, 10, and 12 nm were tested to assess the Gibbs-Thompson effects. Elastic energy contributions were excluded based on previous reports indicating that TSSD corresponds to the thermodynamic solubility limit.

For the precipitation simulations, a single spherical δ-hydride nucleus was nucleated at the center of the domain. Periodic boundary conditions were again imposed for η and c, and zero-displacement Dirichlet boundary conditions were applied to the mechanical fields on all boundaries to remove rigid-body motion. The nucleation was conducted using an order-parameter-only (OPO) seeding method, in which only the non-conserved order parameter is modified while the conserved concentration field remains unchanged.

The precipitation simulations were performed from 525 to 675 K in 25 K increments. At each temperature, we scanned the relaxation factor ψ in increments of 0.1 and identified the minimum bulk hydrogen concentration at which the hydride remained stable and continued to grow. The value of ψ was then selected by calibrating this simulated precipitation threshold to the experimentally measured TSSP at the same temperature.

3. Results

For all interfacial energies and particle radii investigated, the minimum bulk hydrogen concentration required to suppress hydride dissolution increases with temperature. In addition, the dissolution solubility exhibits a clear and systematic sensitivity to the interfacial energy.

At a given temperature and interfacial energy, smaller hydride particles demand higher hydrogen concentrations to remain stable, consistent with a Gibbs-Thomson-type curvature effect. The influence of particle size diminishes as the radius increases; the relative

difference in the required hydrogen concentration falls below 4% for radii of 10-12 nm across all temperatures and interfacial energies considered. On this basis, a hydride radius of 10 nm was adopted for all simulations to define a consistent reference condition while limiting curvature-related size effects.

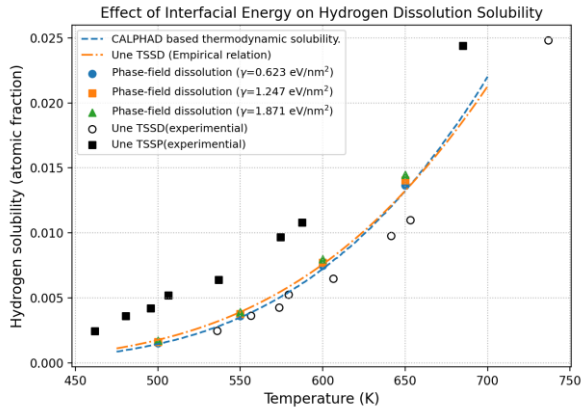

Figure 1. Effect of interfacial energy on hydrogen dissolution solubility

increasing particle radius and remains below 4% for radii between 10 and 12 nm for all temperatures and interfacial energies considered. Based on this assumption, a hydride radius of 10 nm was selected for all simulations, providing a consistent reference condition while minimizing size-related effects.

Precipitation simulations further indicate that elastic

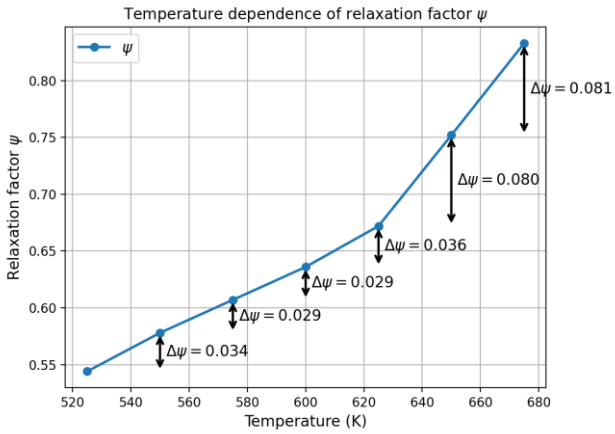

Figure 2. Temperature dependence of relaxation factor ψ

strain energy increases the hydrogen concentration needed for hydride stability, yet elastic effects alone do not reproduce the experimentally reported TSSP. To capture the missing contribution, a temperature-dependent relaxation factor ψ, representing the effect of plastic deformation, was introduced, which enabled quantitative agreement with both the magnitude of TSSP and its temperature dependence. The calibrated ψincreased with temperature (e.g., $\psi = 0.544$at 525 K and $\psi = 0.833$at 675 K). The fitted $\psi(T)$was expressed using a polynomial form, as given in Eq.~(12):

$$\psi(T) = 9.60 \times 10^{-6}T^2 - 9.69 \times 10^{-3}T + 2.995 \quad (12)$$

4. Conclusions and future work

A CALPHAD-informed phase-field framework based on the Kim–Kim–Suzuki (KKS) formulation was developed to evaluate TSSD and TSSP while quantitatively separating the contributions from interfacial energy, elastic strain energy, and plastic relaxation. Dissolution simulations show that the dissolution boundary increases with temperature and interfacial energy, whereas the particle-size effect becomes weak for radii $\gtrsim 10$ nm. Using interfacial energies of 0.623–1.247 eV/nm^2, the predicted TSSD agrees well with the empirical correlation of Une et al.

Precipitation simulations indicate that elastic strain energy increases the hydrogen concentration required for hydride stability, but elasticity alone cannot reproduce the experimentally measured TSSP. Introducing a temperature-dependent relaxation factor to represent plastic deformation enables quantitative reproduction of both the magnitude of TSSP and its temperature dependence.

Future work will focus on assessing the effect of dimensionality. In this study, the simulations were performed in 2D to efficiently capture mechanistic trends; however, the 2D plane-strain setting imposes geometric constraints relative to a fully three-dimensional system, which may shift the absolute TSSP values. A dedicated 3D study will therefore be carried out to quantify the impact of out-of-plane elasticity on TSSP and to confirm the quantitative transferability of the present conclusions.

REFERENCES

[1] A. T. Motta, L. Capolungo, L. Q. Chen, M. N. Cinbiz, M. R. Daymond, D. A. Koss, E. Lacroix, G. Pastore, P. C. A. Simon, M. R. Tonks, B. D. Wirth, M. A. Zikry, Hydrogen in zirconium alloys: A review, Journal of Nuclear Materials 518 (2019) 440–460.

[2] R. Singh, S. Mukherjee, A. Gupta, P. De, S. Banerjee, R. Kameswaran, S. S. Sheelvantra, M. I. Bhabha Atomic Research Centre, Determination of terminal solid solubility of hydrogen in Zr-alloy pressure tube material using dilatometry technique (Jan. 2025).

[3] N. Moelans, B. Blanpain, P. Wollants, An introduction to phase-field modeling of microstructure evolution, Calphad 32 (2) (2008) 268–294.